Long acting anti-infection constructs on titanium

By

Stefano Perni[1,#], Hadil Faris Alotaibi[1,#], Abdulla A.Yergeshov[2], Trinh Dang[2], Timur I. Abdullin[2], Polina Prokopovich[1,*]

[1] School of Pharmacy and Pharmaceutical Sciences, Cardiff University, Cardiff, UK

[2] Institute of Fundamental Medicine and Biology, Kazan (Volga Region) Federal University, 18 Kremlyovskaya St., 420008 Kazan, Russia

[#] these authors contributed equally

* Corresponding author: Dr Polina Prokopovich

School of Pharmacy and Pharmaceutical Sciences

Cardiff University

Redwood Building, King Edward VII Avenue

Cardiff, UK

CF10 3NB

E-mail address: prokopovichp@cf.ac.uk

Abstract

Peri-prosthetic joint infections (PJI) are a serious adverse event following joint replacement surgeries; antibiotics are usually added to bone cement to prevent infection offset. For uncemented prosthesis, alternative antimicrobial approaches are necessary in order to prevent PJI; however, despite elution of drug from the surface of the device being shown one of the most promising approach, no effective antimicrobial eluting uncemented device is currently available on the market. Consequently, there is a clinical need for non-antibiotic antimicrobial uncemented prosthesis as these devices present numerous benefits, particularly for young patients, over cemented artificial joints. Moreover, non-antibiotic approaches are driven by the need to address the growing threat posed by antibiotic resistance.

We developed a multilayers functional coating on titanium surfaces releasing chlorhexidine, a well-known antimicrobial agent used in mouthwash products and antiseptic creams, embedding the drug between alginate and poly-beta-amino-esters.

Chlorhexidine release was sustained for almost 2 months and the material efficacy and safety was proven both in vitro and in vivo. The coatings did not negatively impact osteoblast and fibroblast cells growth and were capable of reducing bacterial load and accelerating wound healing in an excisional wound model.

As PJI can develop weeks and months after the initial surgery, these materials could provide a viable solution to prevent infections after arthroplasty in uncemented prosthetic devices and, simultaneously, help the fight against antibiotic resistance.

1 Introduction

Joint replacement procedures have a very high degree of success; however, as all surgeries, there is a risk for the patients to develop infections. Prosthetic joint infection (PJI) incidence has reported around 1% [1] and 2% [2] and they are one of the most common cause of joint replacement [3]. Beside the highly negative consequences to quality of life [4], and potential reduction of life expectancy; PJI also poses an extremely high economic burden to hospital and health care providers because of the additional hospitalisations, surgical procedures and drugs involved in their treatment [1, 5]. For example, the cost associated to a treating PJI in USA was $70,378 and $56,275 after hip and knee replacement, respectively [6]; similarly in the UK, the estimated cost for PJI after hip arthroplasty was £21,937 [7]. The obvious approach to PJI is prevention; this can be achieved by modifying the surface of implants or incorporating antimicrobial compound(s) onto the device [8].

Joint replacement devices can be classified into cemented and un-cemented depending on the fixation technique. The later requires shorter operating time and has a greater preservation of bone stock facilitating revision [9]; additionally it is not affected by any of the possible complications associated with cemented fixation such as third body wear, retained loose fragments and bone cement implantation syndrome [9, 10].

PJI can develop not just shortly after surgery, but also months and years following device insertion [11-13]. This distinct characteristic, compared to other surgical infections, requires a prolonged antimicrobial activity [8, 14, 15]. Direct conjugation of antimicrobial molecules [16], deposition of drug-loaded nanoporous titanium layers [17], nanodiamonds [18] or single drug eluting coatings [19, 20] on the surface of titanium are examples of the numerous approaches have been attempted to prepare antimicrobial releasing titanium surfaces; these approaches however have not demonstrated antimicrobial activity for prolong period of time as drug release was completed within hours or days, therefore their performance is still not fully satisfactory. The most promising releasing system, in terms of being able to sustain drug elution for extended periods of time, is multilayers coatings; these consist of oppositely

charged polyelectrolytes alternately deposited on the surface of implants [21]; during the deposition, the drug is entrapped between layers and is later released via film-erosion or diffusion [22]. The main advantage of polyelectrolyte multilayers coating is that the amount of drug loaded into the film can be adjusted based on the total number of layered films; moreover, the release kinetic and duration can be tailored using different polyelectrolytes and thus this approach is versatile and amenable to different molecules [23].

The rising threat posed by antibiotic resistance needs also addressing, beside the duration of the antimicrobial activity. Although the majority of studies on anti-infective prosthesis focused on antibiotics such as gentamicin [24-28]; many PJI isolates exhibit resistance to various antibiotics aggravating the concerns surrounding PJI. Silver ability to inactivate microorganisms has been widely researched [29, 30]. However, there are growing concerns related to environmental safety and toxicity, associated to the use metal ions or nanoparticles [31, 32]. Therefore, the use of alternative antimicrobial agents is encouraged [14] and overuse of existing broad-spectrum antibiotic should be avoided [33]. Chlorhexidine is a non-antibiotic antimicrobial agent widely used in mouthwashes, topical antiseptic and intravenous catheters [34, 35]; it has broad spectrum activity and is highly effective against both Gram+ and Gram- bacteria; recently chlorhexidine has been also tried in orthopaedic applications [36] and wound irrigation during arthroplasty [37].

An uncemented device able to prevent PJI over the full product life-cycle and not relying on antibiotics or nanometals has not been produced yet; in this work, we addressed such challenge developing a titanium surface capable of providing antimicrobial activity for months using non-antibiotics drugs. For this purpose, multilayers coatings containing chlorhexidine were prepared on the surfaces of titanium particles used as a model for actual implant devices as the procedure employed to deposit the coating is not affected by the size or shape of the substrate. In this context, the nanoparticles prepared and studied in this work were used as other commonly employed material models such as rods [38-40], disks [41] or wafers [20]; thus we did not envisage depositing the coated nanoparticles onto the surface of devices [42, 43].

The coatings were characterised and drug release kinetic quantified along with the duration of antimicrobial activity; before in-vivo experimentation, the safety of the material was determined through multiple assays on human osteoblasts and fibroblasts; finally the material safety, the ability to reduce bacterial load and accelerate wound healing was validated in an excisional rat wound model.

2 Material and methods

2.1 Chemicals

Titanium (IV) oxide (anatase, < 25nm, 99.7%), (3-Aminopropyl) triethoxysilane (APTS, 99%), chlorhexidine diacetate, 1,6 hexanediol diacrylate, piperazine, sodium alginate, phosphate buffer solution (PBS) tablets, sodium acetate trihydrate (≥99%), brain heart infusion (BHI) agar and broth, Mueller-Hinton (MB) agar and broth, MTT (3-4, 5-dimethylthiazol 2,5-diphenyltetrazolium bromide and In Vitro Toxicology Assay Kit LDH were purchased from Sigma-Aldrich, UK. Dichloromethane (DCM), diethyl ether, dimethyl-sulfoxide (DMSO), ethanol, xylene, HPLC grade acetonitrile, glacial acetic acid and toluene were purchased from Fisher, UK. RPMI-1640 medium, minimum Essential Medium Eagle (MEM), heat-inactivated foetal bovine serum (FBS) and 1% penicillin-streptomycin (PS) were purchased from Gibco by Life Technologies, US.

All chemicals were reagent grade, stored according to manufacturer's guidelines and used as received.

2.2 Titanium surface functionalization and coating

2.2.1 Surface functionalization of titanium oxide nanoparticles

Titanium oxide nanoparticles were functionalized with amino groups via silanation [44, 45]; 1 g of TiO_2 nanoparticles was dispersed in 15 mL of anhydrous toluene and 100 μL of APTS were added to the suspension that was incubated for 24 h at room temperature under constant stirring. The amine functionalized TiO_2 nanoparticles (TiO_2-NH_2) were recovered through centrifugation (14000 rpm at 20 °C

for 5 min (LE-80K Ultracentrifuge, Beckman Coulter, UK)) and subsequent wash in fresh toluene using a vortex mixer (WhirliMixer^{TM}, Fisherbrand, UK). Centrifugation and washing procedure were repeated for further 3 times and then TiO$_2$-NH$_2$ nanoparticles were collected and dried under fume hood for 24 h.

2.2.2 PBAE preparation

Amino-terminated poly-β-amino esters (PBAEs) were synthesised by mixing 3.7 mmol of 1,6 hexanediol diacrylate with a 10% excess of piperazine in 5 mL of DCM (Figure 1a). The polymerization was performed under stirring at 50 C for 48 h. The resulting amino terminated PBAE was precipitated in about 50 mL of diethyl ether and the solvent evaporated under vacuum [46].

2.2.3 Deposition of multi-layers coatings

TiO$_2$-NH$_2$ nanoparticles were coated with polyelectrolyte multilayers. The layers consisted of different numbers of repeating sequence of alginate, chlorhexidine, alginate and PBAE; one sequence containing these four layers were termed quadruple layer (QL) (Figure 1b).

Polyelectrolytes solutions (2 mg/ml for alginate and PBAE and 10 mg/mL for chlorhexidine) were prepared in 0.1 M acetate buffer pH = 5. All solutions were stirred constantly using a magnetic stirrer at 600 rpm for 2 h at 20 °C before use to ensure full dissolution.

The coating procedure was adapted from [44]; typically 1 g of TiO$_2$-NH$_2$ nanoparticles were placed into a test tube and with 20 mL of alginate solution; the mixture was homogenised for 10 min and the nanoparticles were collected by centrifuging at 5000 rpm, 20 °C for 2 min. The alginate-layered nanoparticles were washed with acetate buffer and centrifuged with the supernatant discharged. The second layer was applied dispersing the nanoparticles in 10 mL of chlorhexidine solution. The mixture was homogenised, centrifuged and washed using a similar procedure to that for alginate layer. Further steps of polyelectrolyte coating, centrifugation and washing were repeated for the third layer and fourth layer (alginate and PBAE, respectively), resulting in the first quadruple layer. Layer-by-layer coating process was continued to achieve 10 quadruple layers. During the coating process, a small amount of

coated nanoparticles were collected for evaluation: nanoparticles with one (QL1), three (QL3), five (QL5), seven (QL7) and ten quadruple layers (QL10). After the final washing cycle, TiO_2-NH_2 nanoparticles were collected and dried under fume hood for 24 h.
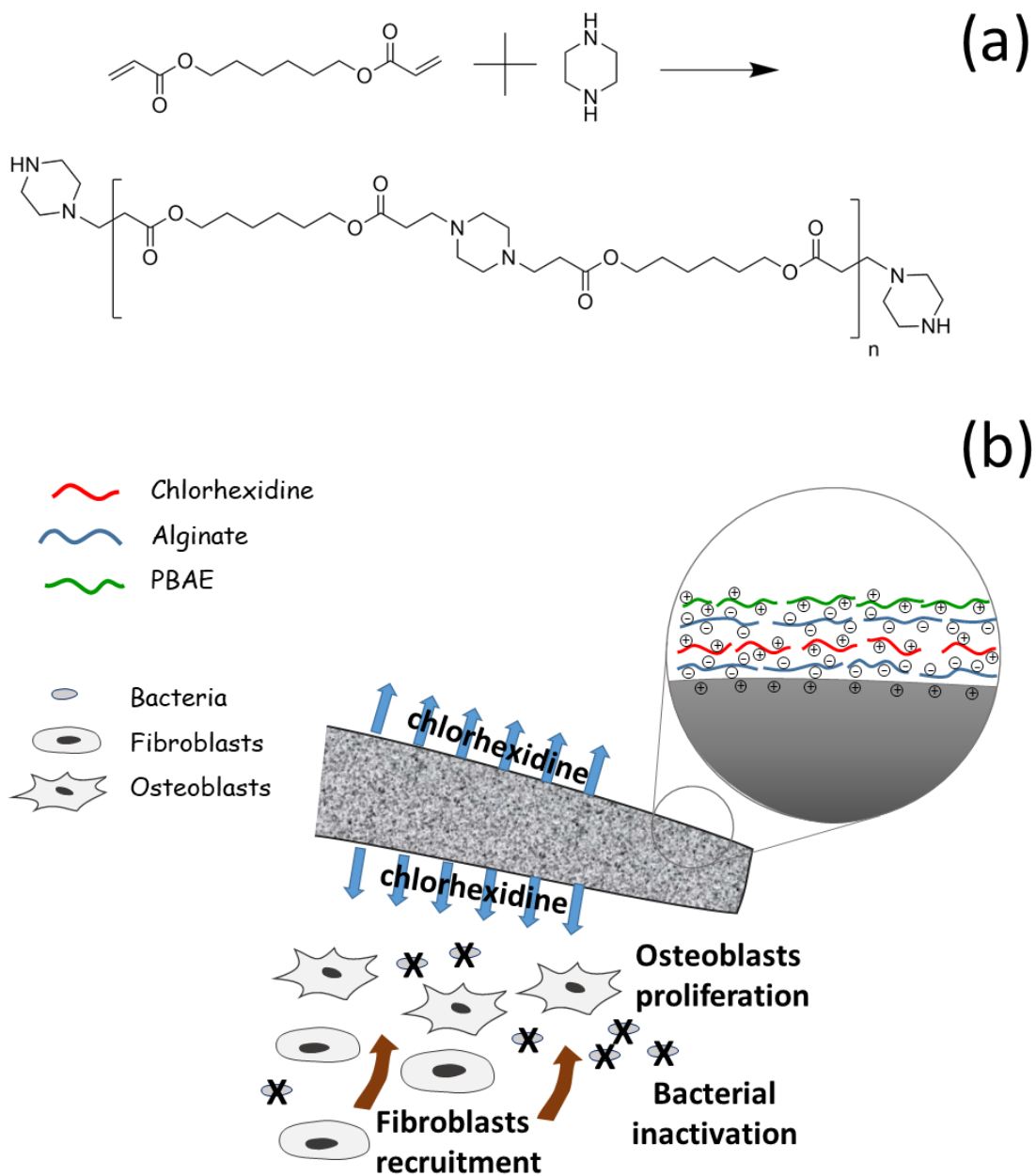
Figure 1. PBAE reaction and structure (a). Schematic representation of chlorhexidine releasing multilayer coating on titanium surfaces and environmental consequences (b).

2.3 Coating characterisation

2.3.1 Transmission Electron microscopy – particle size determination

Images of particles were obtained using a Zeiss 902 transmission electron microscope (TEM) operating at a voltage of 80 kV. The aqueous dispersion of the particles was drop-cast onto a carbon-coated copper grid that was dried at room temperature before loading into the microscope (direct deposition). The average particle size, size-distribution and morphology analysis of the samples was carried out from transmission electron micrographs using ImageJ for Windows (Version 1.50i) [15, 44, 46].

2.3.2 Thermogravimetric Assay (TGA)

Thermogravimetric analysis (TGA) was performed using a Perkin-Elmer TGA 4000 instrument. Coated nanoparticles were initially weighed and heated from 50 to 800 °C with a heating rate of 10 °C/min. Weight loss percentage of each sample at 100 °C and 800 °C were determined relative to initial weight of sample. Organic and inorganic content was determined by subtracting the point at initial weight loss (%) up to when the line plateaus (approximately around 800 °C) [15, 44, 46].

2.3.3 Surface charge

2 mg of nanoparticles were dispersed in 1 mL of acetic buffer (0.1 M) at pH = 5; the ζ potential was measured using Zetasizer ZEN 3600, Nano Series (Malvern, U.K.) through the Smolokowski equation.

2.4 Chlorhexidine release quantification

Coated-particles were dispersed (10 mg/mL) in either acetate buffer pH = 5 or phosphate buffer pH = 7.3, and incubated statically at 37 °C. The medium was withdrawn daily for quantification and the replaced with an equal volume of fresh buffer. All experiments were performed on 3 independent nanoparticles batches.

The amount of chlorhexidine released from the coated nanoparticles was determined using reverse-phase High Performance Liquid Chromatography with a Agilent Technologies® HPLC (1100 series) equipped

with a Waters-Spherisorb ODS2 column (Pore size- 80Å 5 µm and packing dimension of 4.6 mm X 150 mm) and a UV detector at 239 nm. The injection volume was 10 µL while the mobile phase was 0.1 M acetate buffer pH = 5 acetonitrile 58:42 at a flow rate of 1 mL/min.

Stock solutions of chlorhexidine (ranging from 0.4-25 µg/mL) were prepared separately for calibration.

2.4.1   Drug loading estimation

The mass of chlorhexidine loaded into functionalized TiO_2 nanoparticles was estimated by analyzing the supernatant obtained during the centrifugation steps. The collected supernatant was analyzed using HPLC to measure the amount of chlorhexidine which was not loaded over the particles. Chlorhexidine loading % were estimated based on the following equation [47].

$$\text{Drug loading } (\%) = \frac{initial\ drug\ mass - drug\ mass\ left\ in\ the\ supernatant}{initial\ particle\ mass} * 100 \tag{1}$$

This approach was chosen as no suitable solvent was identified to perform the solvent-release approach [48]. Traces of the coatings were still identified on the nanoparticles through TGA, possibly indicating that not all chlorhexidine was extracted. Moreover, the possibility that some drug could have deposited along the walls of the container or on the stir bar was assessed but no decrease in concentration of chlorohexidine in the solution was noticed when no particles were dispersed.

2.5   Antimicrobial testing

The following clinical isolates from PJI were utilised: methicillin-resistant Methicillin resistant *Staphylococcus aureus* (MRSA) 275 and 294; *Staphylococcus epidermidis* 272, 222 and 199; Methicillin resistant *Staphylococcus epidermidis* (MRSE) 140, *Acinetobacter baumannii 646, 643, 640*; *Escherichia coli* 293 and *Enterococcus* 181. Bacteria frozen stokes were stored at -80 °C; strains were streaked on BHI plates weekly and incubated for 24 h at 37 °C, then stored at 4 °C.

Test antimicrobial testing protocol was previously described [27, 28]. A loopful of each bacterial strain was inoculated into BHI broth and incubated statically for 24 h at 37 °C. The cells suspension was diluted

1:1000 in fresh BHI broth and 20 µL of the diluted cells suspension were placed into a sterile 96-well plate. Each well was filled with 100 µL of the release medium from coated titanium nanoparticles corresponding to a set release day, and the plates were incubated for 18-24 h at 37 °C. Growth in each well was evaluated visually. Each experiment was performed in triplicate on independent culture for each individual strain.

2.6   In vitro cell culture assessment

2.6.1   Cells culture

Human osteoblast cells (Saos-2) were purchased from ATCC and grown in RPMI-1640 medium whilst human dermal fibroblast cells were kindly supplied by Prof. Stephens [49] from Cardiff University and grown in Minimum Essential Medium Eagle (MEM). Both media were supplemented with 10% heat-inactivated foetal bovine serum (FBS) and 1% penicillin-streptomycin (PS).

Both cells lines were incubated at 37 °C in a humidified air atmosphere with 5% CO_2; media were changed twice per week.

2.6.2   Exposure of cells to release media containing drug

The release buffer from the first 24 h at pH = 7.3 was sterilised through a 0.22 µm syringe filter and diluted in fresh sterile medium with all supplements in a ratio 1:10. $5 \cdot 10^4$ cells/well were seeded in 96-well plates (Thermo Fisher Scientific, Denmark) and incubated for 24 h at 37 °C in a humidified 5% CO_2 atmosphere to allow cell attachment. After removing the medium, cells were washed with sterile PBS and then incubated with the release media from coated or uncoated nanoparticles, or fresh medium containing pure chlorhexidine at the same concentration of the release medium from coated nanoparticles, for up to 3 days at 37 °C in a humidified atmosphere with 5% CO_2. Cells incubated in fresh medium without release buffer were used as blank control.

2.6.3 Biological tests

20 μL of MTT stock solution (5 mg/mL) and 100 μL of PBS were added to each well and incubated in a humidified atmosphere at 37 °C with 5% CO_2. After 4 h, the supernatant was then removed and 100 μL of dimethyl sulfoxide were added. The absorbance was measured by a spectrophotometer (Lab Tech LT5000MS) at 560 nm; mitochondrial activity was normalised against cell exposed to fresh medium only.

LDH was quantified in the media (LDH released) and after adding the cell lysis solution (LDH total) according to manufacturer's protocols. Total and released LDH (indicated as LDH_{total} and $LDH_{released}$ respectively) were determined as OD, at 490 nm, after correcting for the reading from the negative control. Cell viability was calculated according to the following equation: [45]

$$viability\ (\%) = \frac{LDH_{total} - LDH_{released}}{LDH_{total}} * 100 \tag{2}$$

2.7 In vivo study

Adult male Wistar rats (336 ± 38 g) were received from Vivarium of Academy of Medical and Technical Sciences (Russia). Animal care was performed according to European regulations on the protection of experimental animals (Directive 2010/63/UE) and Russian regulations (No. 742 from 13.11.1984, Ministry of Education and Science). The animals were housed at a temperature of 20 ± 3 °C and a humidity of $65 \pm 10\%$. The surgical study was approved by the Institutional Ethical Review Board of the Kazan Federal University.

2.7.1 Excisional wound model

An excisional wound model was used as detailed previously [50]. The animals were anaesthetized by tiletamine-zolazepam-xylazine intraperitoneal injection (30 - 20 - 10 mg/kg, respectively). The upper back skin of each animal was shaved and cleansed with 70% ethanol solution. Two round full thickness skin excisions were made on the rat back [50] also removing subcutaneous muscle. The excisions were ca. 12 mm in diameter and 2.5 mm in depth and were located 2 cm from each other. To prevent wound closure due to contraction, round silicone splints (internal diameter 12 mm, external diameter 25 mm,

thickness 0.5 mm) were applied around each wound and fixed to the skin using a sterile skin stapler ApposeTM ULC 35W (Covidien). The wounds were disinfected by rinsing with 0.01% miramistine solution (Infamed, Russia) and washed with sterile saline solution.

Staphylococcus aureus (ATCC 29213) pre-grown in Mueller-Hinton (MB) broth was used to infect wounds. A night culture of *S. aureus* was diluted with sterile PBS to obtain a bacterial suspension (10^8 CFU/mL), which was applied and spread on the wound surface (100 µL per wound). Sterile PBS was used as a control solution (for non-infected wounds).

Formulations of either uncoated nanoparticles or coated with 10 quadruple layers (QL10) were prepared right prior the treatment by suspending 3.3 mg of particles in 1 mL sterile PBS in Eppendorf tubes and sonicating the suspension in an ultrasonic water bath for 3 min. 24 h after infection the wounds were treated with the antibacterial formulation or the blank formulation (100 µL per wound per single treatment). Inert non-adhesive polyurethane films (Hydrofilm, Paul Hartman), matching the excision diameter, were attached to the treated wounds to assist spreading and retention of formulations on the wound surface. Finally, adhesive polyurethane films were fixed over the silicone splints to cover the treated wounds. 24 h after infecting, the antibacterial and control formulations were applied to the wounds 3 times each 12 h. The compared formulations were administered to the same animals in order to consider probable variation in immune status of rats and minimize the number of animals used. To assess the infected wounds treated with the antibacterial and blank formulations and control wounds (untreated infected and non-infected) 12 and 6 animals were used, respectively.

2.7.2   Evaluation of wound healing

Wound images were taken using a DP-M17 USB digital microscope.

A wound swab was performed at day 4 after infecting (day 3 after the treatment) by applying 100 µL of sterile saline solution for 1 min and collecting the wound secretion with sterile cotton swabs, which were further transferred into the tube with sterile MH broth to release the bacteria. Bacterial colonies were

quantified by spreading 5 µL of the diluted bacterial inoculum onto MH agar and culturing it at 37 °C. The grown colonies were counted and identified in a random way by a matrix-assisted laser desorption/ionization (MALDI) time-of-flight (TOF) Microflex mass-spectrometer (Bruker Daltonik GmbH).

The animals were sacrificed at days 7 and 14 post-treatment. The wound and surrounding tissues were dissected. The explants were fixed in 4% neutral buffered formalin solution in PBS at room temperature for 48 h, washed, dehydrated in a graded series of ethanol solutions (50, 70, 90, 96 and 100%) and cleared in xylene. The samples were embedded in paraffin blocks and cut on a microtome HM 355S (Thermo Fisher Scientific) into thin sections (7 µm). The tissue sections were subjected to Giemsa and picro-Mallory trichrome staining and analysed by bright-field microscopy on an Axio Observer Z1 microscope (Carl Zeiss).

In order to assess the infection rate in wound tissues, the relative area of bacterial aggregates in Giesma-stained tissue sections was quantified using ImageJ software. In addition, wound contraction rate was estimated as a relative distance between closing wound edges according to histological images; the complete junction corresponds to 100% contraction rate [51].

Doppler flowmetry imaging of the wounds was performed prior to sacrificing animals (at 7 and 14 days) using laser Doppler imaging system (Aïmago SA).

2.8   Statistical analysis

All data were expressed as mean ± standard deviation (SD) from at least three independent values. The comparison of the number of coatings layers impact on the release profiles was carried out fitting a linear model after a logarithmic transformation of the chlorohexidine concentration values, followed by an ANOVA test and Tukey's post hoc test of an individual pair of data sets ($p < 0.05$). Student-t test was performed to determine the impact on antimicrobial activity of individual species. The comparison of the

effects of the chlorohexidine coatings on Saos-2 and fibroblast cells mitochondrial activity and viability
was performed using an ANOVA test.

Statistical analysis of in vivo data was performed using non-parametric Wilcoxon signed rank test or
Student t-test depending on data distribution following Gaussian distribution as determined with the
Shapiro test. All statistical analysis was performed using the R (R Core Team, 2012) [52].

3 Results

3.1 Nanoparticles surface and material characterisation

Particles appeared cubical and spherical-like shaped (Figure 2a to c) with relatively narrow distributed
diameters (Table 1). The coatings did not noticeably impact the size of the particles; however, after 10
quadruple layers, some particles agglomeration could be observed.

Sample	Average diameter (nm) ± SD
TiO_2-particles	34±5
Amino-functionalised particles	34±6
QL10	40±8

Table 1. Average diameter size of TiO_2 nanoparticles bare, after functionalisation and deposition
determined from TEM images

The zeta potential of amino functionalised titanium nanoparticles was +38.4 ± 0.65 mV.

Thermograms of chlorhexidine coated titanium nanoparticles showed a plateau from about 650 °C (Figure
2d). We presumed that the organic content has been lost at this point, and only the inorganic core of the
nanoparticles remained. The total loss of weight at 100 °C represented vaporization of entrapped moisture

in nanoparticles and was not the result of degradation of organic compounds (alginate, PBAE or chlorhexidine). In contrast, the most dramatic weight loss occurred over the range 180 – 230 °C in chlorhexidine coated titanium nanoparticles indicated drug and polymers thermal decomposition. The weight loss of nanoparticles at 800 °C was influenced by the number of quadruple layers. The order of organic content increased with increasing deposited layers (Table 2); moreover, the organic content of bare TiO_2 nanoparticles was the lowest, being 1.44 ± 0.08 %, increasing to 4.48 ± 0.67 % after amino-silanisation.
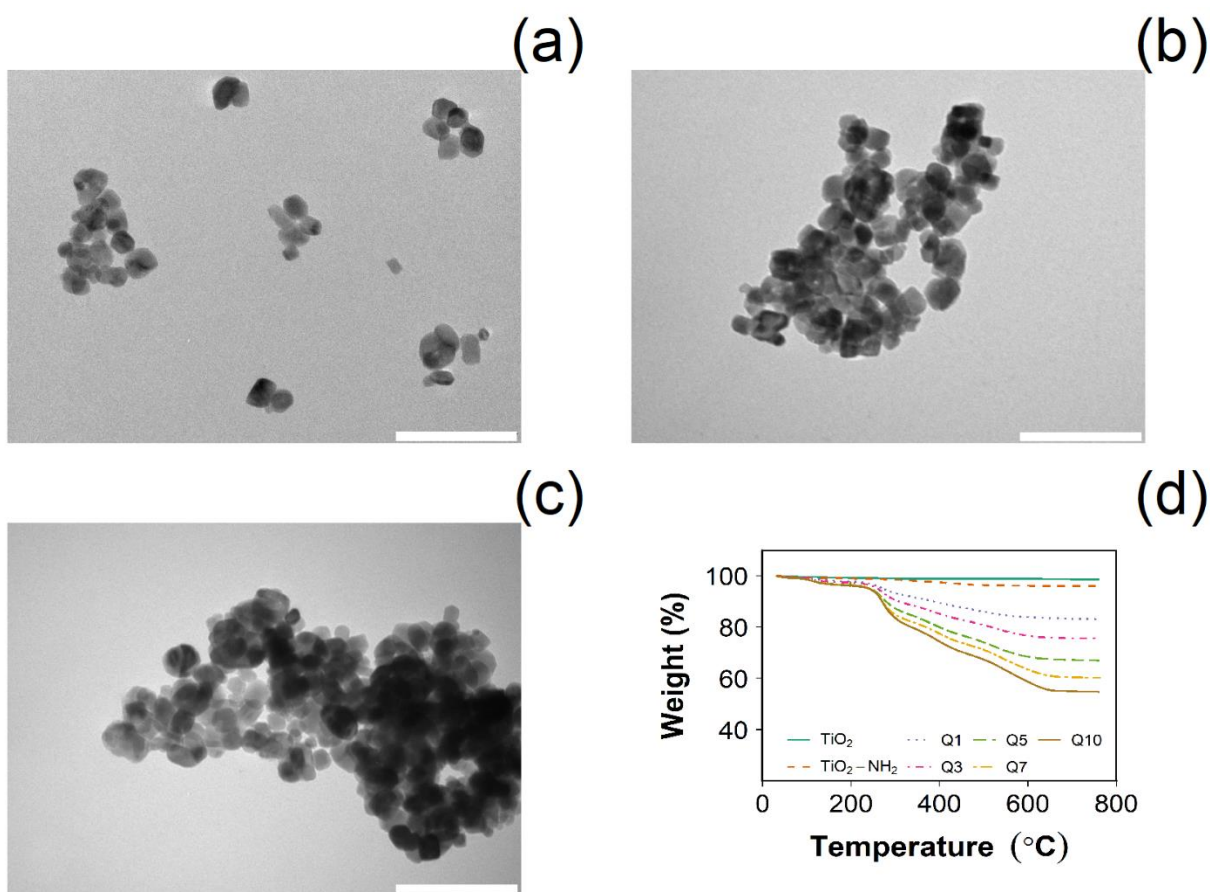
Figure 2. Example of Transmission Electron Microscopy images of (a) bare TiO_2 nanoparticles, (b) amino functionalised (TiO_2-NH_2) nanoparticles and multilayers coated (QL10). Bar represents 100 nm. (d) Thermogravimetric analysis for chlorhexidine layered titanium nanoparticles

NP	% organic content
Core	1.44 ± 0.08
Functionalised	4.48 ± 0.67
QL1	15.37 ± 0.01
QL3	21.55 ± 0.57
QL5	32.38 ± 0.06
QL7	36.41 ± 1.92
QL10	42.23 ± 5.84

Table 2. Organic content (%) in chlorhexidine layered titanium nanoparticles.

3.2 Chlorhexidine release from coatings

The total amount of chlorhexidine released monotonically increased with the number of quadruple layers (Figure 3a and b). Chlorohexidine release from 10 and 7 quadruple layers was detectable for more than 60 days in both conditions. Whereas the chlorhexidine concentration in the release buffer was detectable for 50 days in both pH = 5 and pH = 7.3 when 5 quadruple layers were deposited; furthermore, released chlorhexidine concentration fell below detection limit under 40 days in both release buffers when one or three quadruple layers were deposited. Chlorhexidine coated titanium nanoparticles showed release kinetic decreasing with time and the release rate of chlorhexidine was higher at pH = 5 than at pH = 7.3.

The concentration of chlorhexidine in the buffer followed an exponential decrease (see supp. information).

3.3 Antimicrobial testing

Antimicrobial analysis (Figure 3c) against selected bacterial strains commonly encountered in PJIs was performed only on release medium obtained from titanium nanoparticles coated with 10 quadruple layers as these exhibited the longest release. All the strains tested were also gentamicin resistant (MIC > 500 mg/L).

Growth inhibition of these bacteria was achieved by the release medium, i.e. 4-17 days of release for Gram- (*E. coli* and *A. baumannii*) and 17-28 days for Gram+ (*S. epidermis,* MRSE, MRSA and

Enterococcus), indicating strongest susceptibility of Gram+ towards chlorhexidine. The least sensitive bacteria were the three *A. baumannii* strains tested, where nanoparticles releasing chlorhexidine were able to inhibit growth of *A. baumannii* 643 for 4 days and *A. baumannii* 646 and 640 for 6 days. Growth of *E. coli* 293 and MRSE 140 was inhibited by medium released up to 16 days. Growth of *Enterococcus* was inhibited by medium released up to 18 days while MRSA 924 and MRSA 275, were successfully inhibited by medium released up to 20 days and 28 days, respectively. *S. epidermidis* isolated 199, 222, and 275 were inhibited by medium released up to 23, 25, and 22 days, respectively.
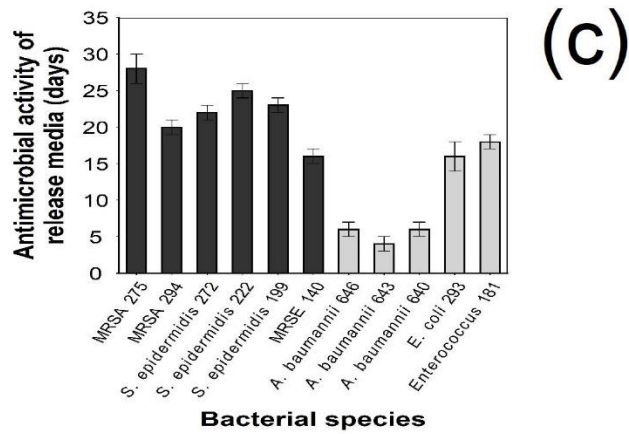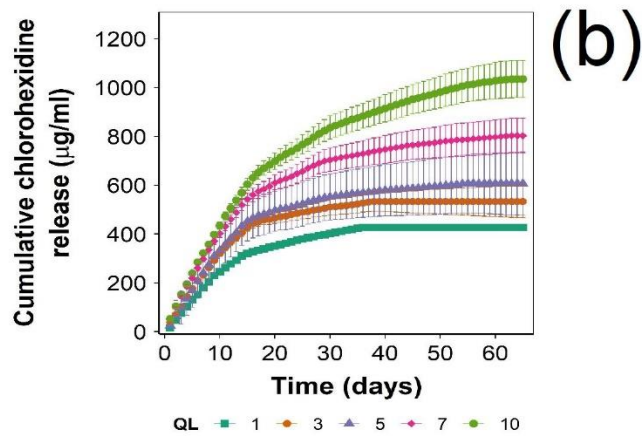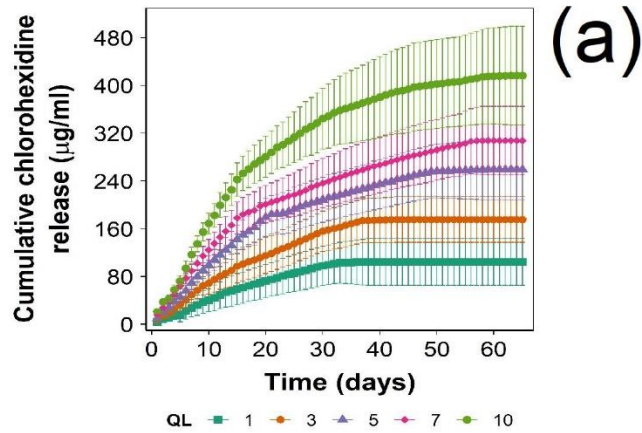
Figure 3. Chlorhexidine cumulative release in acetate buffer pH = 7.3 (a) and pH = 5 (b) from QL1, QL3, QL5, QL7 and QL10 (mean ± SD, n = 3). (c) Antimicrobial testing for 10QL chlorhexidine coated titanium nanoparticles against various PJI clinical isolates (mean ± SD, n=3); black columns for Gram+ and gray for Gram- bacteria.

3.4 MTT and LDH assays

Mitochondrial activity of both human osteoblast and fibroblast cells increased with incubation time; no reduction ($p > 0.05$) in mitochondrial activity of osteoblasts was observed after incubation for up to 4 days (Figure 4a and b) with medium containing the release products of coated or uncoated titanium surfaces compared to cells grown in fresh medium. Similarly, pure chlorhexidine, at the same concentration detected in the release medium from coated titanium surfaces, did not statistically impact mitochondrial activity ($p > 0.05$).

No statistically significant differences ($p > 0.05$) in the viability, assessed through the LDH protocol, of both cells types were observed after incubation for up to 4 days with the release media from the coated or uncoated surfaces compared to samples grown in fresh medium alone or chlorhexidine at the same concentration detected in the release medium from coated titanium surfaces (Figure 4c and d).
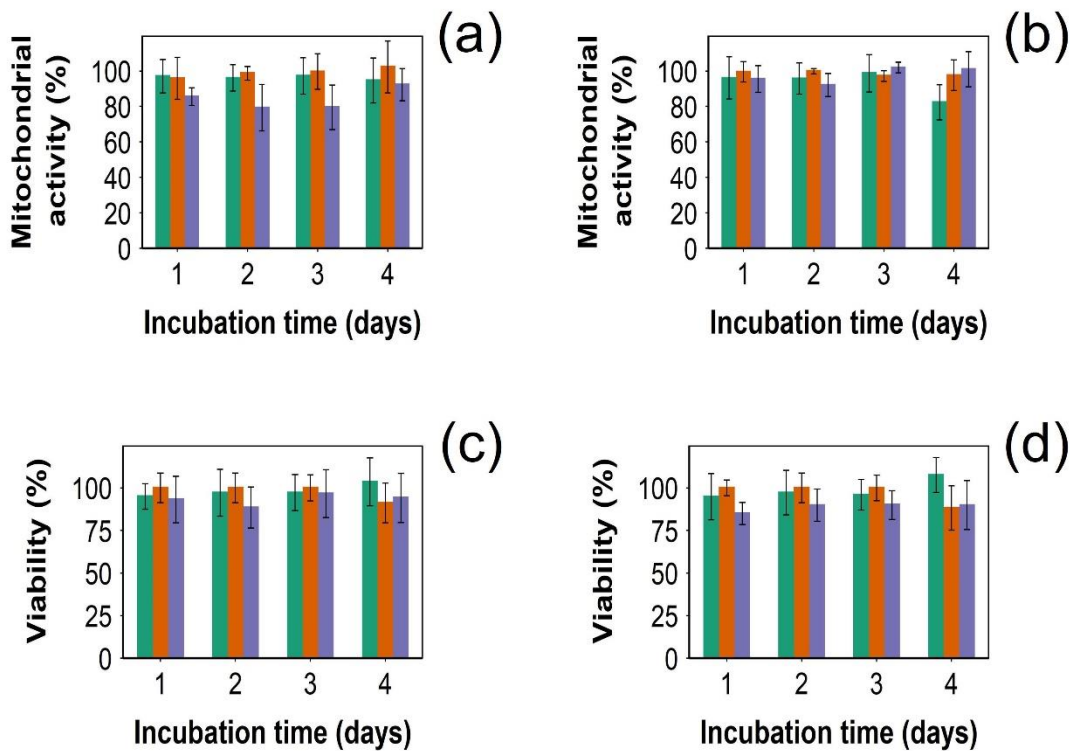
Figure 4. Mitochondrial activity of human osteoblasts (Saos-2) (a) and fibroblasts (b) assessed through MTT assay; viability of human osteoblasts (Saos-2) (c) and fibroblasts (d) assesses through LDH exposed

to medium containing chlorhexidine released from coated titanium surfaces (1:10) for 1, 2, 3 and 4 days (mean ± SD, n = 6). Mitochondrial activity normalised against cell grown for the same incubation time in pure fresh medium. Green columns represent pure chlorhexidine, brown columns uncoated titanium surfaces, blue column represent titanium surfaces with chlorhexidine releasing coatings.

3.5   In vivo validation of antimicrobial activity and material safety

The inoculation of excisional wounds with *S. aureus* was accompanied by the intense formation of a pus substance (Figure 5b) indicating acute bacterial infection. The developed formulations were topically administered one day post-inoculation to allow bacteria to propagate in the wound.

The swab test showed a decrease of the bacteria content in the wash-outs from infected wounds treated with the chlorhexidine releasing coatings compared with the uncoated samples. The statistical analysis showed almost 2-fold significant difference in the corresponding median values (Figure 5e). All detected bacterial colonies belonged to *S. aureus* according to the mass-spectrometry analysis (data not shown), suggesting lack of side contamination. Almost no bacteria were detected in the non-infected wounds under the same conditions.

In addition to bacteria content at the wound surface, Giemsa-stained wound cross-sections were studied to assess the impact of the chlorhexidine releasing coatings on healing of the infected wounds (Figure 6 and Figure 8). Two representative regions in wound cross-sections were analysed: the wound edges which regenerate faster due to cells migration and nutrients supply from surrounding tissues and the central wound region with lower regenerative capacity.
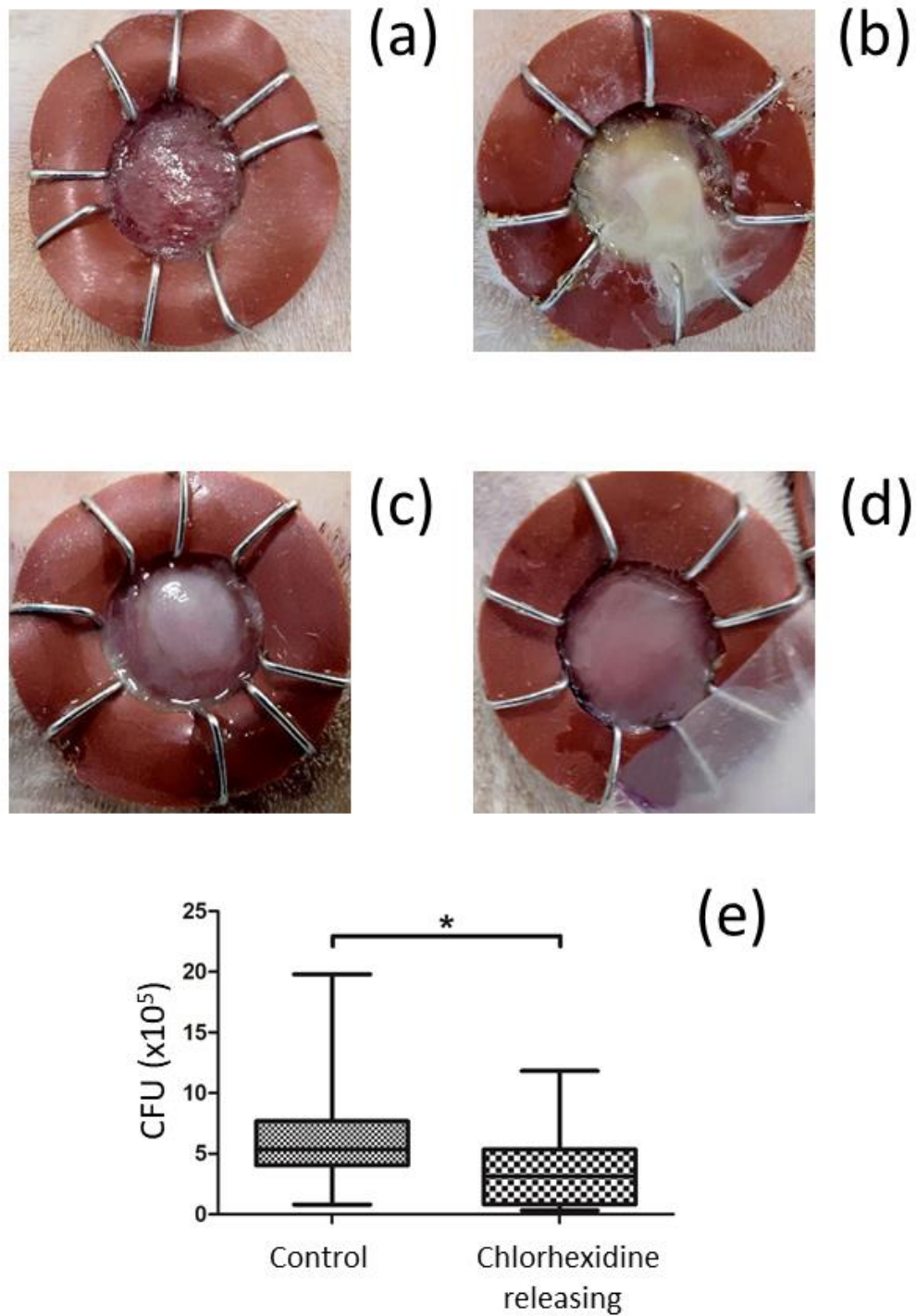
Figure 5. Representative pictures of rat excisional wounds (a) non-infected and (b) infected (both 1 day after applying PBS or *S. aureus*); (c) infected after treatment with non-chlorhexidine releasing surfaces (day 4) and (d) infected after treatment with chlorhexidine releasing coatings (day 4). (e) Median colony forming unit (CFU) values for swabs from infected wound treated with chlorhexidine releasing or control Ti nanoparticles at day 4 (n = 12, * p < 0.05).

In the non-infected wounds typical healing process was observed at days 7 and 14, which corresponded to late inflammatory/early proliferation phases. The skin regeneration was substantially impaired in the infected wounds both untreated and treated with uncoated Ti nanoparticles and only retarded in the chlorhexidine treated infected wounds (in comparison with the non-infected group). In the case of uncoated samples at 7 day, a huge number of bacterial colonies were detected in the fibrous tissues as dark blue aggregates both in the edge and central regions of the wound (Figure 6a and d). At higher magnification, individual bacteria, i.e. greenish round cells less than 1 µm in diameter, and bacterial colonies could be visualized (Figure 6g and h). The number and density of the bacterial colonies was profoundly reduced upon chlorhexidine treatment (Figure 6b and e). The infection rate quantified as a relative area of bacterial colonies in wound cross-sections was 6.3 times lower (p < 0.05) in the case of chlorhexidine releasing formulation compared with the uncoated group (Figure 7c).

In addition, groups of large cells detected throughout the wound tissues (Figure 6) and typically stained with violet color (Figure 6g) are tissue macrophages, which digest bacteria, debris and play an important role in the regulation of immune response [53]. Roundish hollow spaces (e.g. Figure 6e) correspond tolarge adipose cells (removed by organic solvents)which are also involved in inflammatory and regenerative processes [54].

More structured tissues were observed in the chlorhexidine-treated wounds. In the peripheral region the epidermis started to reform, and the regenerating dermis consisted of more mature collagenous tissue (Figure 6b), unlike the wounds treated with the uncoated nanocarriers (Figure 6a). In the central region of the former wounds, the primary fibrous tissue was more developed (Figure 6e and d); this tissue precedes the formation of structured collagen fibers appeared in faster-regenerating non-infected wounds (Figure 6f).

After 14 days, the chlorhexidine treated wounds contained few hardly detectable bacterial colonies (Figure 8b and d). In the case of uncoated samples the bacterial infection was considerably reduced over 7

day but still detected (Figure 7c, Figure 8a). An increase of almost 2 (day 7) and 1.5-fold (day 14) in the

contraction rate of the infected wounds treated with the chlorhexidine releasing formulation over the

uncoated Ti surfaces was also found (Figure 8e). This further supports enhanced feature of the

regeneration of wound tissues in the presence of antibacterial formulation.
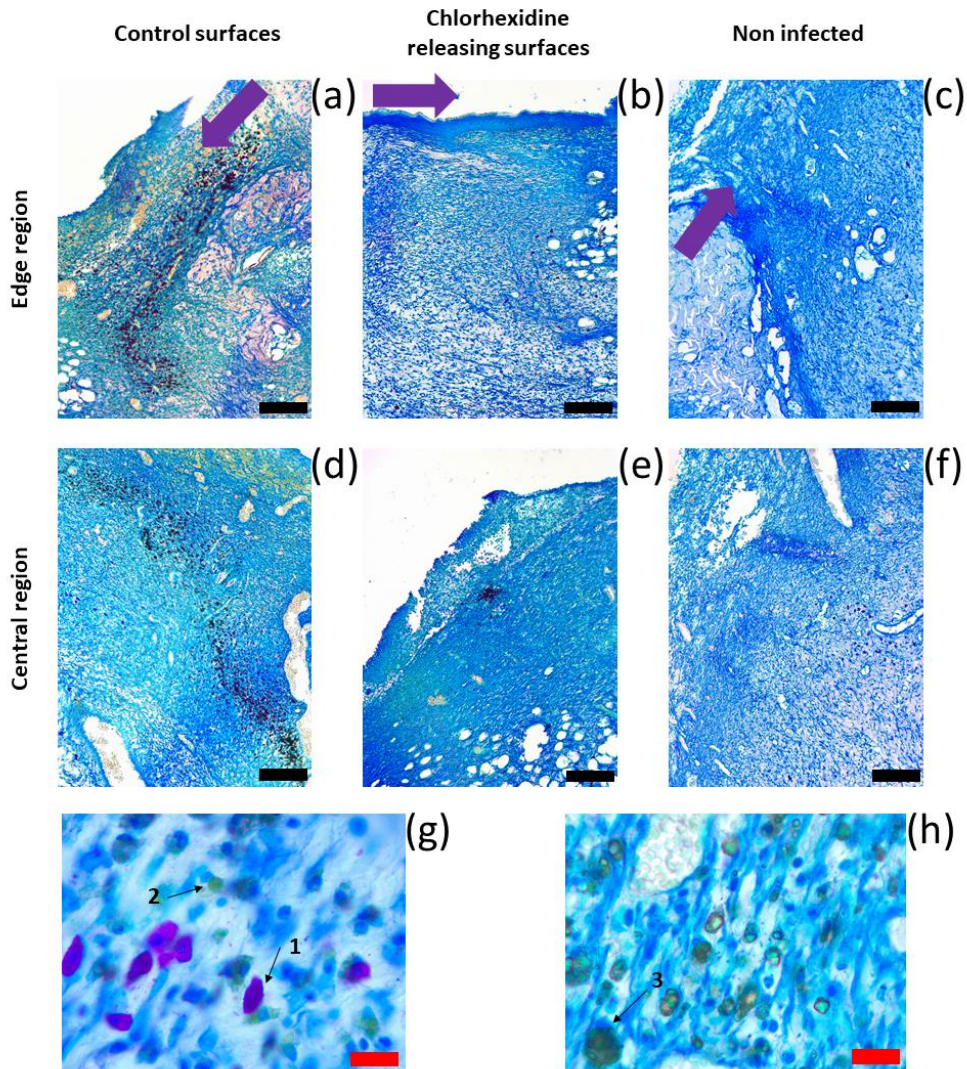
Figure 6. Representative cross-sections of Giemsa-stained wound tissues at day 7. Black bars represent 400 μm, and red bars represent 20 μm. Arrows show the direction of edge tissue growth in the wound. In G and H (uncoated group) typical bacterial colony 1, tissue macrophage 2 and bacterial colony 3 are indicated.
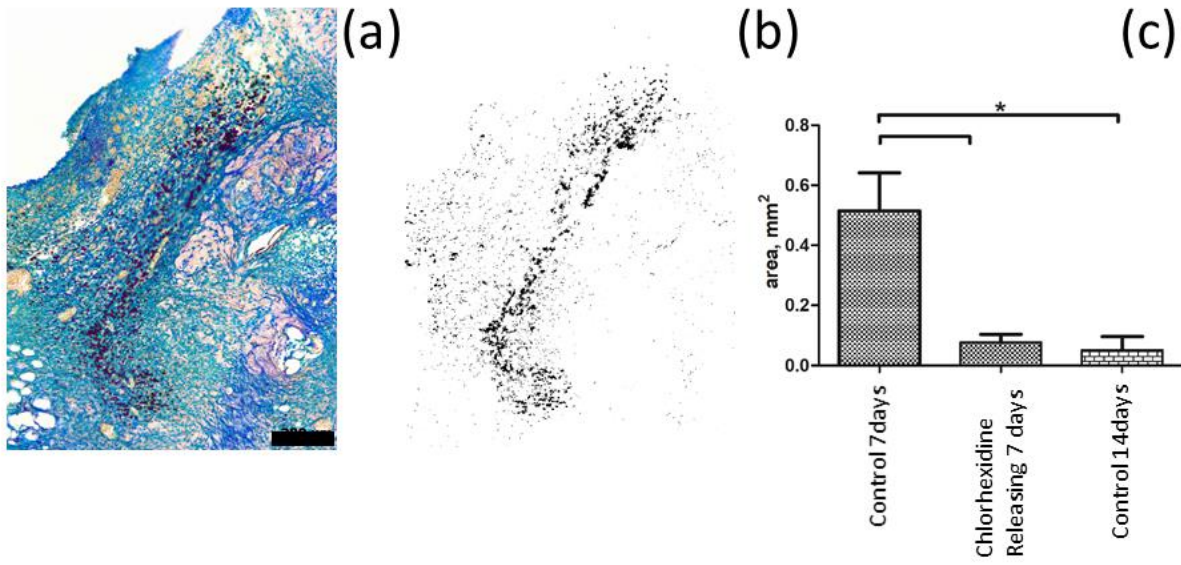
Figure 7. Quantification of infection rate in cross-sections of Giemsa-stained wound tissues. Representative picture of infected wound (a). Highlighting and analysis of bacterial ensembles using Image J software (b). Mean area of bacterial ensembles per wound cross-section ± SD (c). Number of images analysed were 18 for each group (6 animals × 3 typical pictures), *p < 0.05.
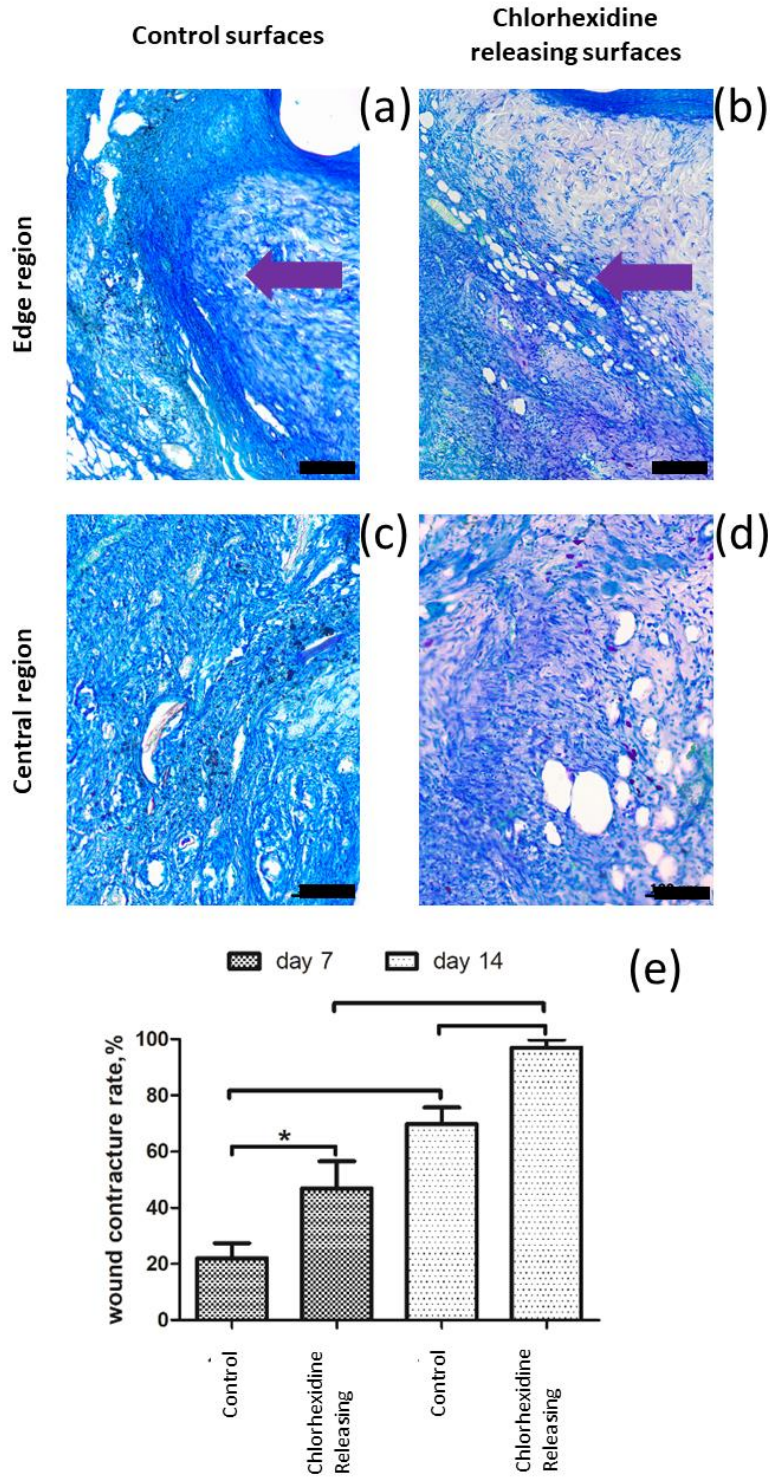
Figure 8. Representative cross-sections of Giemsa-stained wound tissues at day 14 (a–d). Arrows show the direction of edge tissue growth in the wound. Black bars represent 400 μm. (e) Contraction rate (%, mean ± SD) for the wounds treated with chlorhexidine releasing or uncoated samples at day 7 and 14(n = 18, *p < 0.05).

The analysis of wound tissues at day 14 stained by collagen-specific Mallory trichrome method provided similar observations (Figure 9). In the non-chlorhexidine releasing surfaces group collagen fibers (blue) were mainly detected in the peripheral region of the wound (Figure 9a) but not in the central region (Figure 9b); the regenerating dermis/epidermis edges were not closed. In the central region of chlorhexidine treated wounds there were much more structured collagen fibers both more mature (blue) and less mature (red) [55] (Figure 9d), the regenerating dermis/epidermis edges were almost closed, and the epidermis was much better formed (Figure 9c). In non-infected wounds, even more mature dermis was formed (Figure 9e and f).
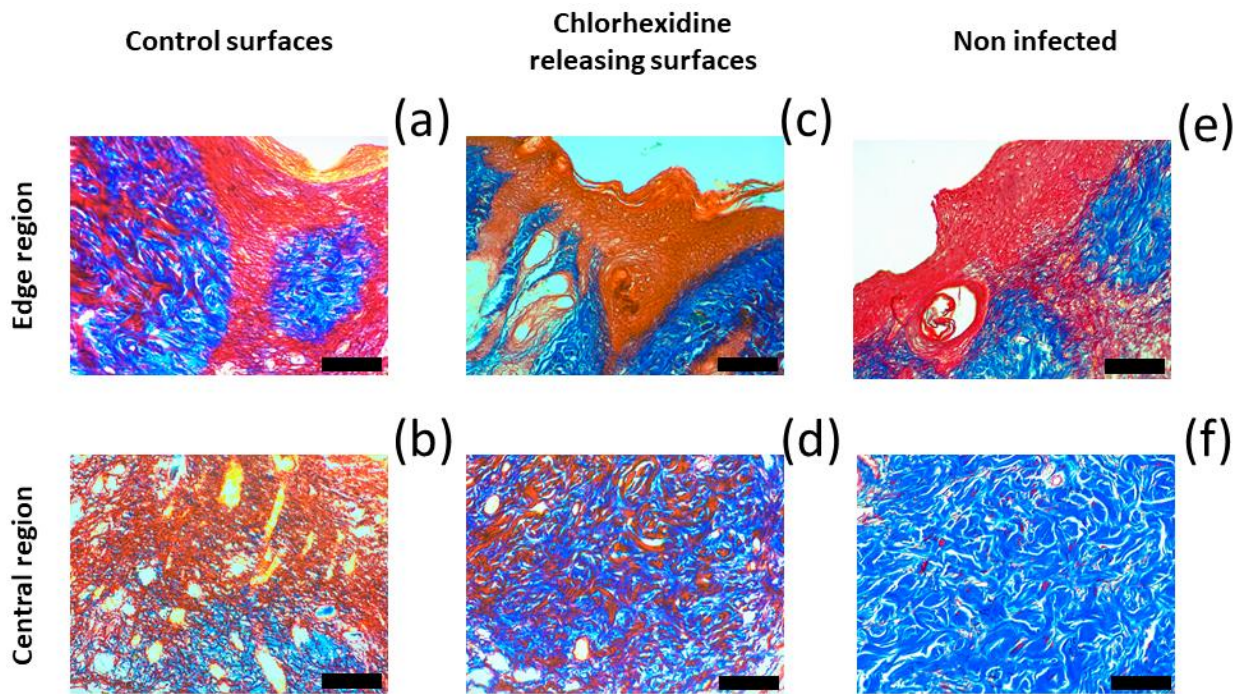
Figure 9. Representative cross-sections of picro-Mallory stained wound tissues at day 14.

The average perfusion rate in the wounds determined using tissue Doppler imaging (Figure 10) significantly differed between the groups (p < 0.05). It increased in proportion of healing process almost doubling from 7 to 14 days in both groups, reflecting the formation of primary blood vessels. Furthermore, for the chlorhexidine releasing surfaces the perfusion rate was noticeably higher than in the uncoated group (Figure 10a).
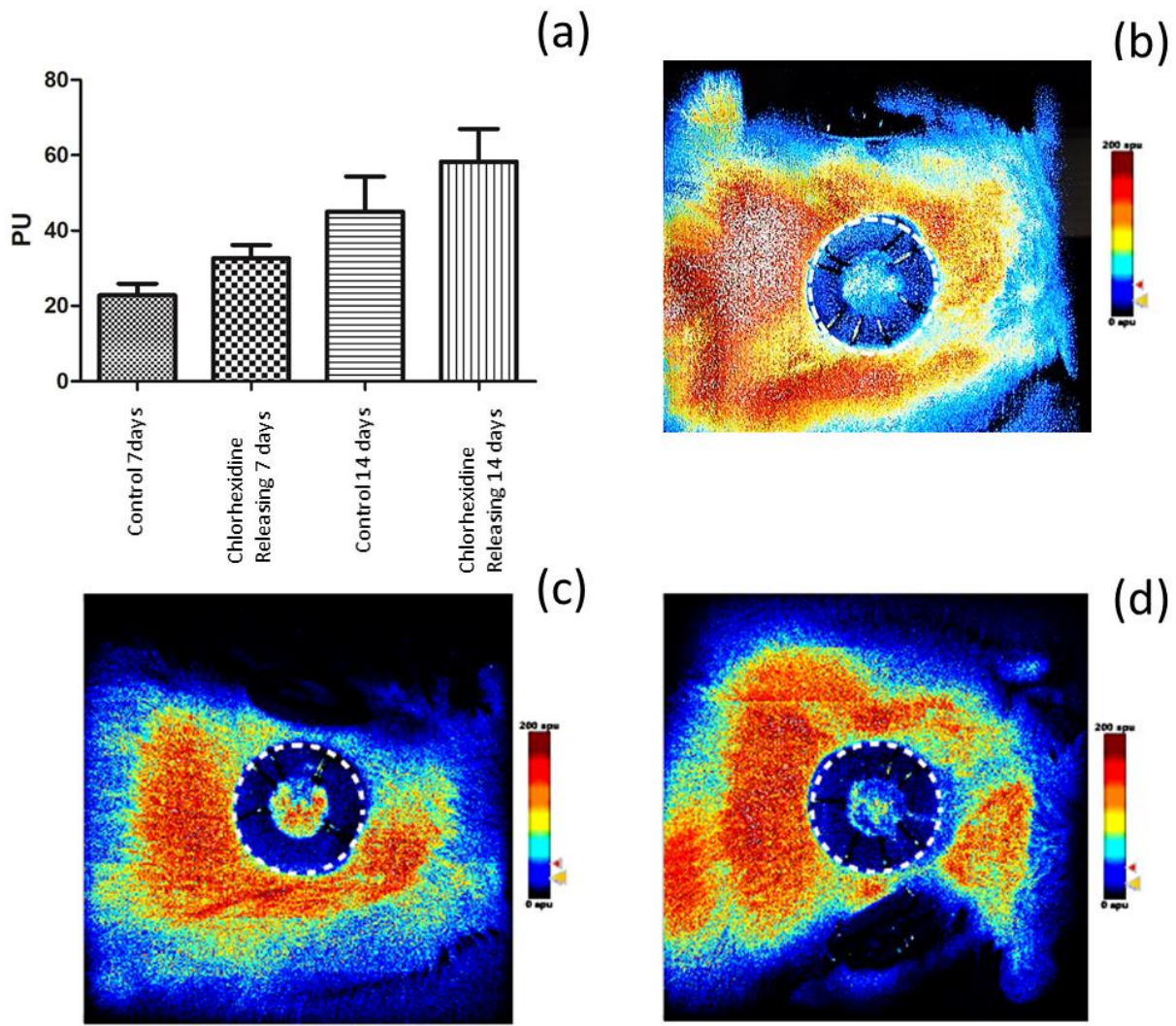
Figure 10. Tissue Doppler imaging analysis of infected wounds treated with chlorhexidine releasing and uncoated surfaces at days 7 and 14. Perfusion rate of wounds in relative perfusion units (mean ± SD, n = 6), p < 0.05 (a). Typical images of skin microcirculation on the back of examined rats treated chlorhexidine releasing surfaces after 7 days (c) and with uncoated samples after 14 days (b) and 7 days (d);

4 Discussion

Infection after joint replacement surgery are a major threat to the log-term success of these procedures; the use uncemented fixation could benefit from the development of titanium surfaces capable of releasing antimicrobial agents. Further considering the growing risk posed by antibiotic resistance, we have developed a multilayers coating on the surface of titanium capable of releasing chlorhexidine for weeks and demonstrated prolonged antimicrobial activity against gentamicin resistant clinical isolates of prosthetic joint infections. Media containing the releasing product of the coating did not impact mitochondrial activity and viability of osteoblasts and fibroblast; safety and efficacy were also validated in vivo.

The surface of titanium carries a nearly neutral charge; consequently to achieve the successful deposition of the first layer of negatively charged alginate, titanium surfaces were functionalized with APTS to present positive charges enabling electrostatic attraction with alginate.

The weight loss at 100 °C was used as a correction in determining organic content [56] as this represented vaporization of entrapped moisture and was not the result of degradation of organic compounds (alginate/PBAE/chlorhexidine). The increase of the total organic content with layers deposited demonstrated the progressive nature of the drug deposition (Table 2); moreover the organic matter in amino functionalized nanoparticles (Table 2) was due to the amino silanol conjugating to the titanium surface. The organic fraction of the nanoparticles after each quadruple layer was close to that reported using the same coating process on silica nanoparticles to deposit gentamicin [46].

The highest dose of chlorhexidine released was ~ 40 mg/L (equivalent to ~ 0.004%) that is about an order of magnitude lower than the toxicity level [57]; moreover repeated exposure to chlorhexidine does not pose an health risk as such molecule is routinely administered daily for oral hygiene.

The release of chlorhexidine was studied in two different conditions (Figure 3a and b) mimicking different physiological situations; the first condition (pH = 5) was mimicking the slightly acidic conditions observed in infected joint [58]. While the other condition (pH = 7.3) represented the healthy joint [59]. Two overlapping mechanisms concur to drug release from multilayers coatings; one is the progressive detachment of the deposited layers (delamination) while the other is the diffusion of the drug through the deposited layers [22]. The observed release kinetic (Figure 3a and b) describes a drug release profile dominated by diffusion as the rate progressively decreases, this is consistent with the results presented for gentamicin [46]; furthermore the observed duration of chlorhexidine release from the coated surfaces was ~ 2 months; hence the technology proposed would be fully capable of providing infection prevention for a period longer than about 1 week as in the case of antibiotic laden bone cement [60]. Moreover, when coatings similar to those employed here are fabricated with gentamicin, drug release had been observed for only 4 weeks [46]. The longer elution achieved with chlorhexidine is likely due to its higher charge and longer chain, compared to gentamicin; both attributes contribute to a lower diffusion through the deposited layers through electrostatic repulsion and sterical hindrance.

In this work, all strains used were gentamicin resistant clinical isolates of PJI and thus represent infections whose management is more complex and costly than those due to gentamicin sensitive species. Antimicrobial testing was carried out directly incubating the release media from the coated nanoparticles with the tested bacteria. This simulates the real scenario in the prosthetic joint surgery. Also only the release media at pH = 7.3 was used as some of the strains were not able to grow sufficiently in the acidic buffer (data not shown). Because uncoated surfaces do not exhibit any antimicrobial activity, the bacterial growth inhibition observed (Figure 3c) was attributable exclusively to the released chlorhexidine from the coatings whose concentration in the media decreased with time (Figure 3a and b). Consequently, the release medium was capable of inhibit growth until chlorhexidine fell below MIC. The different efficacy observed is linked to species and strain variation of MIC; for example MIC for *E. coli* was reported 2.67 µg/mL [61] while for MRSA the MIC was 4-8 µg/mL [62]; *Pseudomonas aeruginosa* is much less

susceptible to chlorhexidine 80 µg/mL [63]. Because of their thin but difficult-to-penetrate cell membrane, Gram- bacteria are often more resistant than Gram+ to antibiotics and other antibacterial interventions [64]; hence, the higher sensitivity of the Gram+ tested in this work is consistent with the general knowledge.

Chlorhexidine, which is widely used in mouthwash solutions and topical treatment, has now been investigated for use in arthroplasty. For example, pins for external fixation coated with hydroxy apatite/chlorhexidine exhibited antimicrobial activity against *S. aureus* in an agar diffusion test [65]. Furthermore, titanium implants with an epoxy based coating releasing chlorhexidine exerted bactericidal effect against *S. aureus* [20]; however, 88% of the loaded drug was released in the first 24 h hence unable to provide antimicrobial activity against only early infections that are only about a third of all PJI [66].

The longer the time between surgery and PJI, the higher is the probability of hematogenic origin of the infection; however the pathogenies of PJI developing in the first year after surgery is still assumed to be primary caused by contaminations during surgery [67] hence it is foreseeable that antimicrobial activity for weeks would reduce the risk of PJI.

The potential adverse local and systemic consequences of topical use of chlorhexidine are little known [36]; however, some detrimental effects have been reported on fibroblasts and osteoblasts [68][69]; therefore, we assessed the impact of the released drug on the viability of various cells encountered in the arthroplasty sites before proceed to experiments in vivo.

We employed two different and complementary assays for the determination of cell viability; because titanium nanoparticles were employed as a model for titanium devices, it was not possible to grow cells directly onto the coated surfaces; hence the response of already established osteoblast cultures to media containing released chlorhexidine was compared to the response to sterile PBS. Moreover, the tests were conducted only from release buffer pH = 7.3 as the acidic buffer (pH = 5) exhibited toxic activity.

Titanium surfaces are used in orthopaedic devices because osteoblast cells are capable of adhering and proliferating on such material thus the high mitochondrial activity observed in the uncoated samples (Figure 4) was well expected; moreover the presence of chlorhexidine from the coatings did not negatively impact osteoblasts and such these materials are not inferior to standard titanium in regards to osteoblast growth. Because titanium, as mentioned, exhibits sufficient cytocompatibility towards osteoblasts it was not necessary for the coatings to improve such properties and proof of non-inferiority was deemed sufficient. The absence of cytotoxicity exhibited by the coatings developed here is in contrast with observations using similar concentration of chlorhexidine [68, 69]; a possible explanation could be our chlorhexidine solution were in basal media instead of PBS and it is possible that the media could provide protection against the action of chlorhexidine or support cell recovery. Furthermore, our in vivo results did not report any negative impact on tissues when chlorhexidine was released from surfaces in contact with such tissues as also reported for epoxy-based coatings [20].

4.1 Wound healing activity of coatings

In order to assess the ability of the coatings to safely perform the designed antimicrobial activity in vivo, a model of infection in rodents was employed. Wound healing in rodents is substantially promoted by tissue contraction unlike human wounds. The excisional model employed utilizing wound splinting has been shown to minimize wound contraction while allowing wound healing to occur through the processes of granulation and re-epithelialization thus providing a more relevant model [70].

The histological data on Giemsa staining, which is routinely used to detect bacteria in tissues [71], confirmed the effective wound infiltration with the *Staphylococcus* infection and suggested a profound direct antibacterial effect of the chlorhexidine containing coatings in contact with the infected wounds (Figure 7). Furthermore, the results showed that the histological analysis of the infected wounds provides more informative evaluation of the course of infection than the swab test. Decreased difference in the bacteria content in wound swabs taken from chlorhexidine and uncoated samples (Figure 5e over Figure 7c) may result from the redistribution of infiltrated and survived bacteria following therapy into

superficial wound layers. The rat organism almost coped with the *Staphylococcus* infection without chlorhexidine treatment at day 14 (Figure 7c). The histological analysis of the bacteria in wounds should be therefore performed during first 14 days following infection; 7 day period provides proper comparison of the untreated and treated wounds in terms of both bacteria content and tissue regeneration efficiency (Figure 6 and Figure 7). The model employed should be suitable for studying acute infections that are those more likely to benefit from a prolonged release of antimicrobial agents after surgery.

The rate of leucocyte infiltration in the wound tissues was visually estimated as follows: chlorhexidine releasing surfaces treated wounds > non-infected wounds > non-chlorhexidine releasing surfaces treated wounds. The differences presumingly reflect both the current phase of wound healing and the direct effect on bacteria. The decreased infiltration of leucocyte of the non-infected wounds over the chlorhexidine treated infected wounds suggests that the former (non-infected) wounds go through the inflammation phase faster. However, the non-supressed bacteria in the untreated infected wounds expectedly oppose to leucocytes and other cells involved in the regeneration by different mechanisms. In particular, *S. aureus* was reported to inhibit released chemokines, adhesion molecules and pro-inflammatory cytokines during wound healing [72]. Therefore, during 7-14 days the persisted infection in the untreated wounds apparently impairs the normal inflammatory process required for the effective skin regeneration. Due to the suppression of bacteria by the long acting chlorhexidine formulation, the healing of infected wounds becomes normal but only retarded over the non-infected process. In comparison with non-chlorhexidine releasing surfaces, the developed antibacterial formulation profoundly promotes the regeneration of infected wounds (Figure 6 and Figure 8). The histological analysis suggests that the healing time of infected wounds reduced to about half by using the chlorhexidine releasing formulation; and such an efficacy is apparently achieved by sustained localized delivery of the antibacterial agent using the nanocarrier.

In addition, the therapeutic efficacy of the developed formulation was confirmed by imaging of blood microcirculation. Although, the full skin excision was accompanied by a disappearance of the skin

microvasculature, the perfusion signal gradually restored (Figure 10a) due to the formation of new vessel-like structures reaching approximately 30-50% of initial values to 14 day after the antibacterial treatment. The perfusion rate is in good agreement with histological data on the regeneration of epidermis and dermis (Figure 6 and Figure 8) including maturation of collagen fibers (Figure 9).

5 Conclusion

We constructed a drug eluting system for non-antibiotic agent (chlorhexidine) for titanium using multilayers coatings. Chlorhexidine release was sustained for about two months without observing detrimental effects osteoblasts and fibroblasts viability.

The results obtained in the in vivo model of wound infection prove that the long-acting formulation does not show side effects in contact with forming skin tissues and is capable of effectively reducing the bacterial load in infected wounds, thus substantially promoting dermis and epidermis regeneration and restoration of skin microcirculation. Overall the system developed can be a solution to the problem of prolonged antimicrobial activity in un-cemented prostheses and antibiotic resistance once further validation of the coated implant ability to promote/support bone integration will be verified.

6 Acknowledgements

7 Data Availability

The raw/processed data required to reproduce these findings cannot be shared at this time due to technical or time limitations.

8 References

[1] E. Alp, F. Cevahir, S. Ersoy, A. Guney, Incidence and economic burden of prosthetic joint infections in a university hospital: A report from a middle-income country, Journal of Infection and Public Health 9(4) (2016) 494-498.

[2] S.M. Kurtz, E. Lau, H. Watson, J.K. Schmier, J. Parvizi, Economic burden of periprosthetic joint infection in the United States, J Arthroplasty 27(8 Suppl) (2012) 61-5.e1.

[3] E. Lenguerrand, M.R. Whitehouse, A.D. Beswick, S.A. Jones, M.L. Porter, A.W. Blom, Revision for prosthetic joint infection following hip arthroplasty, 6(6) (2017) 391-398.

[4] P. Helwig, J. Morlock, M. Oberst, O. Hauschild, J. Hübner, J. Borde, N.P. Südkamp, L. Konstantinidis, Periprosthetic joint infection--effect on quality of life, Int Orthop 38(5) (2014) 1077-1081.

[5] A. Sousa, A. Carvalho, C. Pereira, E. Reis, A.C. Santos, M. Abreu, D. Soares, R. Fragoso, S. Ferreira, M. Reis, R. Sousa, Economic Impact of Prosthetic Joint Infection - an Evaluation Within the Portuguese National Health System, J Bone Jt Infect 3(4) (2018) 197-202.

[6] S.M. Kurtz, E. Lau, J. Schmier, K.L. Ong, K. Zhao, J. Parvizi, Infection burden for hip and knee arthroplasty in the United States, J Arthroplasty 23(7) (2008) 984-91.

[7] I.S. Vanhegan, A.K. Malik, P. Jayakumar, S. Ul Islam, F.S. Haddad, A financial analysis of revision hip arthroplasty: the economic burden in relation to the national tariff, The Journal of bone and joint surgery. British volume 94(5) (2012) 619-23.

[8] M.A. Getzlaf, E.A. Lewallen, H.M. Kremers, D.L. Jones, C.A. Bonin, A. Dudakovic, R. Thaler, R.C. Cohen, D.G. Lewallen, A.J. van Wijnen, Multi-disciplinary antimicrobial strategies for improving orthopaedic implants to prevent prosthetic joint infections in hip and knee, Journal of orthopaedic research : official publication of the Orthopaedic Research Society 34(2) (2016) 177-86.

[9] A. Aprato, S. Risitano, L. Sabatini, M. Giachino, G. Agati, A. Massè, Cementless total knee arthroplasty, Annals of translational medicine 4(7) (2016) 129-129.

[10] A.J. Donaldson, H.E. Thomson, N.J. Harper, N.W. Kenny, Bone cement implantation syndrome, British journal of anaesthesia 102(1) (2009) 12-22.

[11] A.J. Tande, R. Patel, Prosthetic joint infection, Clin Microbiol Rev 27(2) (2014) 302-345.

[12] K. Huotari, M. Peltola, E. Jämsen, The incidence of late prosthetic joint infections: a registry-based study of 112,708 primary hip and knee replacements, Acta Orthop 86(3) (2015) 321-325.

[13] W. Zimmerli, A. Trampuz, P.E. Ochsner, Prosthetic-joint infections, The New England journal of medicine 351(16) (2004) 1645-54.

[14] R. Williams, P. Mihok, J. Murray, Novel Antibiotic delivery and Novel Antimicrobials in Prosthetic Joint infection, 2016.

[15] Y. Al Thaher, S. Perni, P. Prokopovich, Nano-carrier based drug delivery systems for sustained antimicrobial agent release from orthopaedic cementous material, Advances in colloid and interface science 249 (2017) 234-247.

[16] N. Masurier, J.B. Tissot, D. Boukhriss, S. Jebors, C. Pinese, P. Verdié, M. Amblard, A. Mehdi, J. Martinez, V. Humblot, G. Subra, Site-specific grafting on titanium surfaces with hybrid temporin antibacterial peptides, Journal of materials chemistry. B 6(12) (2018) 1782-1790.

[17] M. Jarosz, A. Pawlik, M. Szuwarzyński, M. Jaskuła, G.D. Sulka, Nanoporous anodic titanium dioxide layers as potential drug delivery systems: Drug release kinetics and mechanism, Colloids and surfaces. B, Biointerfaces 143 (2016) 447-454.

[18] E. Krok, S. Balakin, J. Jung, F. Gross, J. Opitz, G. Cuniberti, Modification of titanium implants using biofunctional nanodiamonds for enhanced antimicrobial properties, Nanotechnology 31(20) (2020) 205603.

[19] F. Ordikhani, M. Dehghani, A. Simchi, Antibiotic-loaded chitosan-Laponite films for local drug delivery by titanium implants: cell proliferation and drug release studies, Journal of materials science. Materials in medicine 26(12) (2015) 269.

[20] M. Riool, A.J. Dirks, V. Jaspers, L. de Boer, T.J. Loontjens, C.M. van der Loos, S. Florquin, I. Apachitei, L.N. Rijk, H.A. Keul, S.A. Zaat, A chlorhexidine-releasing epoxy-based coating on titanium implants prevents Staphylococcus aureus experimental biomaterial-associated infection, European cells & materials 33 (2017) 143-157.

[21] H.F. Alotaibi, Y. Al Thaher, S. Perni, P. Prokopovich, Role of processing parameters on surface and wetting properties controlling the behaviour of layer-by-layer coated nanoparticles, Current Opinion in Colloid & Interface Science 36 (2018) 130-142.

[22] R.C. Smith, M. Riollano, A. Leung, P.T. Hammond, Layer-by-layer platform technology for small-molecule delivery, Angewandte Chemie (International ed. in English) 48(47) (2009) 8974-7.

[23] P.T. Hammond, Building biomedical materials layer-by-layer, Materials Today 15(5) (2012) 196-206.

[24] J.S. Moskowitz, M.R. Blaisse, R.E. Samuel, H.P. Hsu, M.B. Harris, S.D. Martin, J.C. Lee, M. Spector, P.T. Hammond, The effectiveness of the controlled release of gentamicin from polyelectrolyte multilayers in the treatment of Staphylococcus aureus infection in a rabbit bone model, Biomaterials 31(23) (2010) 6019-30.

[25] L. Pichavant, G. Amador, C. Jacqueline, B. Brouillaud, V. Héroguez, M.-C. Durrieu, PH-controlled delivery of gentamicin sulfate from orthopedic devices preventing nosocomial infections, Journal of controlled release : official journal of the Controlled Release Society 162 (2012) 373-81.

[26] J. Min, R.D. Braatz, P.T. Hammond, Tunable staged release of therapeutics from layer-by-layer coatings with clay interlayer barrier, Biomaterials 35(8) (2014) 2507-2517.

[27] Y. Al Thaher, L. Yang, S.A. Jones, S. Perni, P. Prokopovich, LbL-assembled gentamicin delivery system for PMMA bone cements to prolong antimicrobial activity, PLOS ONE 13(12) (2018) e0207753.

[28] S. Perni, S. Caserta, R. Pasquino, S.A. Jones, P. Prokopovich, Prolonged Antimicrobial Activity of PMMA Bone Cement with Embedded Gentamicin-Releasing Silica Nanocarriers, ACS Applied Bio Materials 2(5) (2019) 1850-1861.

[29] A. Besinis, S.D. Hadi, H.R. Le, C. Tredwin, R.D. Handy, Antibacterial activity and biofilm inhibition by surface modified titanium alloy medical implants following application of silver, titanium dioxide and hydroxyapatite nanocoatings, Nanotoxicology 11(3) (2017) 327-338.

[30] R. Kuehl, P.S. Brunetto, A.-K. Woischnig, M. Varisco, Z. Rajacic, J. Vosbeck, L. Terracciano, K.M. Fromm, N. Khanna, Preventing Implant-Associated Infections by Silver Coating, Antimicrobial Agents and Chemotherapy 60(4) (2016) 2467-2475.

[31] B. Smolkova, M. Dusinska, A. Gabelova, Nanomedicine and epigenome. Possible health risks, Food and Chemical Toxicology 109 (2017) 780-796.

[32] I. Mahapatra, J.R.A. Clark, P.J. Dobson, R. Owen, I. Lynch, J.R. Lead, Expert perspectives on potential environmental risks from nanomedicines and adequacy of the current guideline on environmental risk assessment, Environmental Science: Nano 5(8) (2018) 1873-1889.

[33] NICE, Antimicrobial stewardship: systems and processes for effective antimicrobial medicine use. NG15, (2015).

[34] K.S. Lim, P.C. Kam, Chlorhexidine--pharmacology and clinical applications, Anaesthesia and intensive care 36(4) (2008) 502-12.

[35] A. Khoo, P. Oziemski, Chlorhexidine impregnated central venous catheter inducing an anaphylatic shock in the intensive care unit, Heart, lung & circulation 20(10) (2011) 669-70.

[36] J. George, A.K. Klika, C.A. Higuera, Use of Chlorhexidine Preparations in Total Joint Arthroplasty, J Bone Jt Infect 2(1) (2017) 15-22.

[37] N.B. Frisch, O.M. Kadri, T. Tenbrunsel, A. Abdul-Hak, M. Qatu, J.J. Davis, Intraoperative chlorhexidine irrigation to prevent infection in total hip and knee arthroplasty, Arthroplasty today 3(4) (2017) 294-297.

[38] J. Chen, Y. Zhu, M. Xiong, G. Hu, J. Zhan, T. Li, L. Wang, Y. Wang, Antimicrobial Titanium Surface via Click-Immobilization of Peptide and Its in Vitro/Vivo Activity, ACS Biomaterials Science & Engineering 5(2) (2019) 1034-1044.

[39] B. Nie, en, T. Long, H. Ao, J. Zhou, T. Tang, B. Yue, Covalent Immobilization of Enoxacin onto Titanium Implant Surfaces for Inhibiting Multiple Bacterial Species Infection and In Vivo Methicillin-Resistant Staphylococcus aureus Infection Prophylaxis, Antimicrobial Agents and Chemotherapy 61(1) (2017) e01766-16.

[40] Z. Yuan, S. Huang, S. Lan, H. Xiong, B. Tao, Y. Ding, Y. Liu, P. Liu, K. Cai, Surface engineering of titanium implants with enzyme-triggered antibacterial properties and enhanced osseointegration in vivo, Journal of Materials Chemistry B 6(48) (2018) 8090-8104.

[41] R. Chen, M.D. Willcox, K.K. Ho, D. Smyth, N. Kumar, Antimicrobial peptide melimine coating for titanium and its in vivo antibacterial activity in rodent subcutaneous infection models, Biomaterials 85 (2016) 142-51.

[42] E. Baghdan, S.R. Pinnapireddy, H. Vögeling, J. Schäfer, A.W. Eckert, U. Bakowsky, Nano spray drying: A novel technique to prepare well-defined surface coatings for medical implants, Journal of Drug Delivery Science and Technology 48 (2018) 145-151.

[43] N.J. Wood, H.F. Jenkinson, S.A. Davis, S. Mann, D.J. O'Sullivan, M.E. Barbour, Chlorhexidine hexametaphosphate nanoparticles as a novel antimicrobial coating for dental implants, Journal of Materials Science: Materials in Medicine 26(6) (2015) 201.

[44] H.F. Alotaibi, S. Perni, P. Prokopovich, Nanoparticle-based model of anti-inflammatory drug releasing LbL coatings for uncemented prosthesis aseptic loosening prevention, International journal of nanomedicine 14 (2019) 7309-7322.

[45] M.C. Rivera, S. Perni, A. Sloan, P. Prokopovich, Anti-inflammatory drug-eluting implant model system to prevent wear particle-induced periprosthetic osteolysis, International journal of nanomedicine 14 (2019) 1069-1084.

[46] Y. Al Thaher, S. Latanza, S. Perni, P. Prokopovich, Role of poly-beta-amino-esters hydrolysis and electrostatic attraction in gentamicin release from layer-by-layer coatings, Journal of Colloid and Interface Science 526 (2018) 35-42.

[47] S. Papadimitriou, D. Bikiaris, Novel self-assembled core-shell nanoparticles based on crystalline amorphous moieties of aliphatic copolyesters for efficient controlled drug release, Journal of controlled release : official journal of the Controlled Release Society 138(2) (2009) 177-84.

[48] C.W. Shields, J.P. White, E.G. Osta, J. Patel, S. Rajkumar, N. Kirby, J.-P. Therrien, S. Zauscher, Encapsulation and controlled release of retinol from silicone particles for topical delivery, Journal of Controlled Release 278 (2018) 37-48.

[49] I.B. Wall, R. Moseley, D.M. Baird, D. Kipling, P. Giles, I. Laffafian, P.E. Price, D.W. Thomas, P. Stephens, Fibroblast dysfunction is a key factor in the non-healing of chronic venous leg ulcers, The Journal of investigative dermatology 128(10) (2008) 2526-40.

[50] D. Luong, A.A. Yergeshov, M. Zoughaib, F.R. Sadykova, B.I. Gareev, I.N. Savina, T.I. Abdullin, Transition metal-doped cryogels as bioactive materials for wound healing applications, Materials Science and Engineering: C 103 (2019) 109759.

[51] H.K. Nagar, A.K. Srivastava, R. Srivastava, M.L. Kurmi, H.S. Chandel, M.S. Ranawat, Pharmacological Investigation of the Wound Healing Activity of Cestrum nocturnum (L.) Ointment in Wistar Albino Rats %J Journal of Pharmaceutics, 2016 (2016) 8.

[52] R Core Team, R: A language and environment for statistical computing. R Foundation for Statistical Computing, Vienna, Austria., 2013.

[53] C.M. Minutti, J.A. Knipper, J.E. Allen, D.M.W. Zaiss, Tissue-specific contribution of macrophages to wound healing, Seminars in Cell & Developmental Biology 61 (2017) 3-11.

[54] S. Borgeaud, L.C. Metzger, T. Scrignari, M. Blokesch, The type VI secretion system of Vibrio cholerae fosters horizontal gene transfer, 347(6217) (2015) 63-67.

[55] N. Lemo, G. Marignac, E. Reyes-Gomez, T. Lilin, O. Crosaz, E. Dm, Cutaneous reepithelialization and wound contraction after skin biopsies in rabbits: A mathematical model for healing and remodelling index, Veterinarski Arhiv 80 (2010) 637-652.

[56] P. Du, X. Zhao, J. Zeng, J. Guo, P. Liu, Layer-by-layer engineering fluorescent polyelectrolyte coated mesoporous silica nanoparticles as pH-sensitive nanocarriers for controlled release, Applied Surface Science 345 (2015) 90-98.

[57] D.E. Freeman, J.A. Auer, Chapter 9 - Instrument Preparation, Sterilization, and Antiseptics, in: J.A. Auer, J.A. Stick (Eds.), Equine Surgery (Fourth Edition), W.B. Saunders, Saint Louis, 2012, pp. 98-111.

[58] T.J. Kinnari, J. Esteban, N.Z. Martin-de-Hijas, O. Sánchez-Muñoz, S. Sánchez-Salcedo, M. Colilla, M. Vallet-Regí, E. Gomez-Barrena, Influence of surface porosity and pH on bacterial adherence to hydroxyapatite and biphasic calcium phosphate bioceramics, Journal of Medical Microbiology 58(1) (2009) 132-137.

[59] M. Ribeiro, F.J. Monteiro, M.P. Ferraz, Infection of orthopedic implants with emphasis on bacterial adhesion process and techniques used in studying bacterial-material interactions, Biomatter 2(4) (2012) 176-94.

[60] M.C. Swearingen, J.F. Granger, A. Sullivan, P. Stoodley, Elution of antibiotics from poly(methyl methacrylate) bone cement after extended implantation does not necessarily clear the infection despite susceptibility of the clinical isolates, Pathogens and disease 74(1) (2016) ftv103.

[61] C.V. do Amorim, C.E. Aun, M.P. Mayer, Susceptibility of some oral microorganisms to chlorhexidine and paramonochlorophenol, Brazilian oral research 18(3) (2004) 242-6.

[62] B.D. Cookson, M.C. Bolton, J.H. Platt, Chlorhexidine resistance in methicillin-resistant Staphylococcus aureus or just an elevated MIC? An in vitro and in vivo assessment, Antimicrobial agents and chemotherapy 35(10) (1991) 1997-2002.

[63] L. Thomas, A.D. Russell, J.Y. Maillard, Antimicrobial activity of chlorhexidine diacetate and benzalkonium chloride against Pseudomonas aeruginosa and its response to biocide residues, Journal of applied microbiology 98(3) (2005) 533-43.

[64] L.K. Siu, Antibiotics: action and resistance in gram-negative bacteria, Journal of microbiology, immunology, and infection = Wei mian yu gan ran za zhi 35(1) (2002) 1-11.

[65] E.S. DeJong, T.M. DeBerardino, D.E. Brooks, B.J. Nelson, A.A. Campbell, C.R. Bottoni, A.E. Pusateri, R.S. Walton, C.H. Guymon, A.T. McManus, Antimicrobial efficacy of external fixator pins coated with a lipid stabilized hydroxyapatite/chlorhexidine complex to prevent pin tract infection in a goat model, The Journal of trauma 50(6) (2001) 1008-14.

[66] K.L. Ong, S.M. Kurtz, E. Lau, K.J. Bozic, D.J. Berry, J. Parvizi, Prosthetic joint infection risk after total hip arthroplasty in the Medicare population, J Arthroplasty 24(6 Suppl) (2009) 105-9.

[67] A.J. Tande, R. Patel, Prosthetic joint infection, Clin Microbiol Rev 27(2) (2014) 302-45.

[68] M. Giannelli, F. Chellini, M. Margheri, P. Tonelli, A. Tani, Effect of chlorhexidine digluconate on different cell types: A molecular and ultrastructural investigation, Toxicology in Vitro 22(2) (2008) 308-317.

[69] J.X. Liu, J. Werner, T. Kirsch, J.D. Zuckerman, M.S. Virk, Cytotoxicity evaluation of chlorhexidine gluconate on human fibroblasts, myoblasts, and osteoblasts, J Bone Jt Infect 3(4) (2018) 165-172.

[70] R.D. Galiano, V. Michaels, Joseph, M. Dobryansky, J.P. Levine, G.C. Gurtner, Quantitative and reproducible murine model of excisional wound healing, 12(4) (2004) 485-492.

[71] G. Tian, Y. Qiu, Z. Qi, X. Wu, Q. Zhang, Y. Bi, Y. Yang, Y. Li, X. Yang, Y. Xin, C. Li, B. Cui, Z. Wang, H. Wang, R. Yang, X. Wang, Histopathological Observation of Immunized Rhesus Macaques with Plague Vaccines after Subcutaneous Infection of Yersinia pestis, PloS one 6 (2011) e19260.

[72] S. Ryu, P.I. Song, C.H. Seo, H. Cheong, Y. Park, Colonization and infection of the skin by S. aureus: immune system evasion and the response to cationic antimicrobial peptides, International journal of molecular sciences 15(5) (2014) 8753-72.